JACS
JOURNAL OF THE AMERICAN CHEMICAL SOCIETY
Article
pubs.acs.org/JACS

A Dinuclear Cobalt Complex Featuring Unprecedented Anodic and Cathodic Redox Switches for Single-Molecule Magnet Activity

Skye Fortier,[†] Jennifer J. Le Roy,[‡] Chun-Hsing Chen,[†] Veacheslav Vieru,[§] Muralee Murugesu,*[,‡] Liviu F. Chibotaru,*[,§] Daniel J. Mindiola,*[,†,∥] and Kenneth G. Caulton*[,†]

[†]Department of Chemistry, Indiana University, 800 East Kirkwood Avenue, Bloomington, Indiana 47405, United States
[‡]Department of Chemistry, University of Ottawa, Ottawa, Ontario KIN 6N5, Canada
[§]Division of Quantum and Physical Chemistry, Katholieke Universiteit Leuven, Celestijnenlaan 200F, B-3001 Heverlee, Belgium

Supporting Information

ABSTRACT: One-electron oxidation or reduction of the paramagnetic dinuclear Co(II) complex $dmp_2Nin\{Co[N(SiMe_3)_2]\}_2$ (**1**; dmp_2Nin^{2-} = bis(2,6-dimethylphenyl)nindigo), by fully reversible chemical or electrochemical methods, generates the radical salts $[\mathbf{1}(OEt_2)]^+$ and $[\mathbf{1}]^-$, respectively. Full structural and magnetic analyses reveal the locus of the redox changes to be nindigo-based, thus giving rise to ligand-centered radicals sandwiched between two paramagnetic and low-coordinate Co(II) centers. The presence of these sandwiched radicals mediates magnetic coupling between the high-spin ($S = {}^3/_2$) cobalt ions, which gives rise to single-molecule magnet (SMM) activity in both the oxidized ($[\mathbf{1}(OEt_2)]^+$) and reduced ($[\mathbf{1}]^-$) states. This feature represents the first example of a SMM exhibiting fully reversible, dual "ON/OFF" switchability in both the cathodic and anodic states.

1. INTRODUCTION

Molecules which exhibit a marked magnetic hysteresis, or "magnetic memory," in the presence of a varying magnetic field are classified as single-molecule magnets (SMMs). The activity of SMMs is distinct from that of classical magnets, as the locus of their magnetic behavior lies completely at the molecular level, independent from that of the bulk material. Since the seminal discovery of SMM activity in the mixed-valence metal cluster $[Mn_{12}O_{12}(OAc)_{16}(H_2O)_4]\cdot 2HOAc\cdot 4H_2O$ (HOAc = CH_3CO_2H) in 1991,[1] SMMs have been extensively investigated owing to their potential for use in advanced magnetic materials and quantum computing devices.[2] In order for SMM activity to manifest itself, a molecule must display both a large magnetic anisotropy, resulting from molecular uniaxial zero-field splitting (D), and a non-negligible spin ($S \neq 0$) ground state. Additionally, the relaxation barrier (U) is directly correlated to the spin value of the molecule, i.e. $U = S^2|D|$ or $U = (S^2 - 1/4)|D|$ for integer and noninteger spins, respectively,[3] and thus complexes with large spins as well as anisotropy are desirable for impeding magnetic spin reversal.

While there is no single synthetic method for designing SMMs, the predominant approach involves generating high-spin systems through the synthesis of polynuclear clusters possessing strongly coupled high-spin paramagnetic metal ions.[4] This is often achieved via self-assembly in one-pot reactions through which a metal precursor is mixed with a multidentate ligand in a carrier solvent. A notable disadvantage of this method is that coordination geometries, crucial to magnetic anisotropy, and solvation spheres can be difficult to predict or control and the process requires a certain amount of serendipity.[3b,4a,5] An alternate approach, which in recent years has gained traction, targets less complicated SMMs through the synthesis of smaller mono- and multinuclear metal systems.[6] When site-directing or sterically encumbering ligands are employed, greater control over the coordination environment can be used to produce systems with highly anisotropic ground states.[3a,6a,7] While this does place a limit on the total possible S value, spins can be modulated by use of organic radicals as noninnocent ligands. Indeed, ligands with radical character that can join metal ions are often used to enhance exchange interactions, especially between lanthanide ions in dinuclear species.[6a,c,8]

Utilizing noninnocent ligands in SMMs offers the enticing possibility for redox *controllable* magnetic behavior, especially the ability for fully reversible "ON/OFF" switchable SMMs. Switchable SMMs would be valuable for use in advanced magnetic applications (e.g., high-density magnetic storage, magnetic thin films) by which their activity could be externally controlled.[2b,9] Moreover, redox-active (noninnocent) ligands offer the ability to move beyond single spin state (e.g., nitroxyl) linkers. To date, only *one* switchable SMM has thus far been reported, namely the redox-active $[(PY5Me_2)_4Mn_4Re(CN)_7](PF_6)_5\cdot 6H_2O$ ($PY5Me_2$ = 2,6-bis(1,1-bis(2-pyridyl)ethyl)-pyridine), by Long and co-workers.[10] In the $[Mn_4Re]^{12+}$ cluster, the manganese ions are centrally bridged by a spin-active $[Re^{IV}(CN)_7]^{3-}$ ($S = {}^1/_2$) core which allows for magnetic exchange interactions within the cluster, an SMM in the "ON"

Received: May 26, 2013
Published: August 30, 2013

   dx.doi.org/10.1021/ja405284t | J. Am. Chem. Soc. 2013, 135, 14670−14678

position. However, upon reduction, the magnetic exchange pathway is deactivated, or turned "OFF" by an $S = 0$ $[Re^{III}(CN)_7]^{4-}$ bridge. Finally, cyclic voltammetric analysis reveals the one-electron redox event to be electrochemically reversible. This remarkable result, while rare, clearly demonstrates the feasibility of redox-induced switchable SMMs but also highlights the challenges associated in choosing ligands which enable such behavior.

Herein, we report a dinuclear cobalt complex supported by a modular binucleating, redox-active ligand capable of existing in *four* different redox states which features fully redox-switchable SMM activity controlled through *both* one-electron reduction and oxidation processes. This system has the advantages of employing an earth-abundant 3d metal, using a dinuclear core, and employing a redox-active organic component.

2. MATERIALS AND METHODS

2.1. Synthesis. All air- and moisture-sensitive operations were performed in an M. Braun Lab Master drybox under an atmosphere of purified nitrogen or using high-vacuum standard Schlenk techniques. Anhydrous hexanes and *n*-pentane were purchased from Sigma-Aldrich in a Sure-Seal reservoir (18 L) and dried by passage through activated alumina and a Q-5 column. Et_2O was distilled, under nitrogen, from sodium benzophenone ketyl and stored over sodium metal and activated 4 Å molecular sieves. [Fc][BAr^f] (Fc = Cp_2Fe^+; BAr^f = B(3,5-$(CF_3)_2C_6H_3)_4$)[11] and complexes **1**, [$K(DME)_4$][**1**], and [$K(Et_2O)_2$]$_2$[**1**] were synthesized as reported.[12] All other reagents were obtained from commercial sources and used as received. NMR spectral data were recorded on a Varian Inova 400 MHz spectrometer. ^{1}H NMR spectra are referenced to $SiMe_4$ (0.0 ppm) using the residual ^{1}H solvent peaks as internal standards. ^{19}F NMR spectra are externally referenced to $CFCl_3$ (0.0 ppm). UV−vis−near-IR spectra were recorded on a Varian Cary 5000 spectrophotometer.

*Synthesis of [dmp$_2$Nin{Co[N(SiMe$_3$)$_2$](Et$_2$O)}$_2$][BAr^f] ([**1**(OEt$_2$)$_2$][BAr^f]).* To a cold (−37 °C) stirred suspension of **1** (0.126 g, 0.139 mmol) in Et_2O (10 mL) was added [Fc][BAr^f] (0.145 g, 0.138 mmol) as a solid. Upon addition, the solution turned dark purple. The solution was immediately layered with hexanes (10 mL) and stored at −37 °C, at which time dark purple crystals were deposited. The crystals were washed with pentane and dried under vacuum, yielding pure material (0.198 g, 74% yield). Note: the complex [**1**$(OEt_2)_2$][BAr^f] decomposes slowly over several hours upon standing in solution at room temperature. Attempts to obtain satisfactory elemental analysis data was unsuccessful, as the values were consistently low in carbon, which we attribute to decomposition resulting from the thermal sensitivity of the compound. ^{1}H NMR (400 MHz, 25 °C, THF-d_8): δ −20.16 (s, 2H), −19.38 (s, 2H), −13.00 (s, 4H), 1.08 (t, 12H, Et_2O), 3.36 (q, 8H, Et_2O), 7.40 (s, 4H, *p*-$(CF_3)_2C_6H_3$), 7.60 (s, 8H, *o*-$(CF_3)_2C_6H_3$), 14.68 (br s, 48H, overlapping *Me N*-aryl and N$SiMe_3$ resonances), 43.61 (s, 2H), 119.26 (br s, 4H). ^{19}F{^{1}H} NMR (376 MHz, 25 °C, THF-d_8): δ −63.35 (s, 24F, B(CF_3)$_2$$C_6H_3$). UV−vis−near-IR ($Et_2O$, 0.10 mM, 25 °C, ε in L mol^{-1} cm^{-1}): 517 (ε = 7822), 688 (sh, ε = 9865), 754 (ε = 11593), 973 nm (ε = 3715).

2.2. X-ray Diffraction. Data for [**1**$(OEt_2)_2$][BAr^f] were collected on a Bruker KAPPA APEX II Duo diffractometer equipped with an APEX II CCD detector. The data collection was carried out using Mo Kα radiation (graphite monochromator). A randomly oriented region of reciprocal space was surveyed to achieve complete data with a redundancy of 4. Sections of frames were collected with 0.50° steps in ω and φ scans. The crystal was mounted on a Mitigen Kapton loop, coated in NVH oil, and maintained at 150(2) K under a flow of nitrogen gas during data collection. Data collection and cell parameter determinations were conducted using the SMART program.[13] Integration of the data and final cell parameter refinements were performed using SAINT[14] software with data absorption correction implemented through SADABS.[15] All hydrogen atom positions were idealized and rode on the atom of attachment. Structure solution, refinement, graphics, and creation of publication materials were performed using SHELXTL.[16] Data can be found at the CCDC, depository no. 921215.

One of the trifluoromethyl groups of the [B(3,5-$(CF_3)_2C_6H_3)_4$]$^-$ anion of [**1**$(OEt_2)_2$][BAr^f] exhibits rotational disorder. The disorder of the trifluoromethyl group was modeled over three positions with 33% occupancy each.

2.3. Cyclic Voltammetry. Cyclic voltammetric measurements were performed using an E2 Epsilon potentiostat with a PC unit controlled by Bioanalytical Systems (BAS) software. Experiments were performed under an inert atmosphere using platinum working and counter electrodes with a Ag/AgCl pseudoreference electrode in a one-compartment cell. Solutions contained approximately 0.1 mM in metal complex with [Bu_4N][PF_6] (0.1 M, THF) as supporting electrolyte. All potentials are reported versus the $[Cp_2Fe]^{0/+}$ couple, referenced as internal standard at 0.0 V.

2.4. Magnetic Measurements. The magnetic susceptibility measurements were obtained using a Quantum Design MPMS-XL7 SQUID magnetometer operating between 1.8 and 300 K for dc (direct current) applied fields ranging from −7 to 7 T. dc analyses were performed on polycrystalline samples of 21, 30, 35, and 24 mg of **1**, [$K(DME)_4$][**1**], [$K(Et_2O)_2$]$_2$[**1**], and [**1**$(OEt_2)_2$][BAr^f], respectively, restrained and sealed in an air-free holder under a field ranging from 0 to 7 T between 1.8 and 300 K. Alternating current (ac) susceptibility measurements were carried out under an oscillating ac field of 3 Oe and ac frequencies ranging from 1 to 1500 Hz. Magnetization data were collected at 100 K to check for ferromagnetic impurities but were found to be absent in all samples. Diamagnetic corrections were applied for the sample holder and the core diamagnetism from the sample (estimated with Pascal constants).

2.5. Ab Initio Calculations. The ab initio calculations were done using the Molcas 7.8 program package.[17] The Cholesky decomposition threshold was set to 0.5×10^{-7}. First, a complete active space self consistent field (CASSCF) calculation was run to account for static correlation energy.[18] Then a complete active space second-order perturbation theory (CASPT2) calculation was carried out to consider the dynamic correlation energy,[19] with an imaginary shift of 0.1 in order to avoid the intruder states. Each cobalt ion was computed by replacing the *neighboring* cobalt ion with zinc. The active space was set to 7 d electrons in 10 orbitals, to take into consideration the double-shell effect.[20] The terms obtained in CASSCF/CASPT2 calculations were further used in the restricted active space state interaction (RASSI) for calculating the effect of spin−orbit interaction (Table S4, Supporting Information). All quartet and doublet states were mixed by the spin−orbit interaction, resulting in 120 spin−orbit multiplets. The SINGLE_ANISO program was used to compute the local magnetic properties on a single metal fragment.[21] The exchange interaction was included by the Lines model within the subroutine POLY_ANISO.[22]

The calculations were done in two geometry approximations: (A) a truncated geometry of fragments (Figure S23, Supporting Information) and (B) the experimental structure with replaced metal ions. Two basis sets have been employed (Table S3, Supporting Information).

3. RESULTS AND DISCUSSION

3.1. Synthesis. We have recently been investigating the chemistry of late 3d transition metals supported by *N*,*N*′-diaryl-*β*-diketimines.[12] These ligands, better known as "nindigo," are formed by two conjoined iminoindole units creating a molecule with bilateral binding sites. The steric and geometric features of each site approximate the coordination environment provided by the architecture of *β*-diketiminates, a highly popular class of site-directing, chelating ligands.[23] Synthesized in good yields through the condensation of amines with indigo dye,[24] the nindigo platform, like *β*-diketiminates, is highly modular, which allows for easy steric tunability. However, unlike *β*-diketiminates, nindigo is distinguished by its rich redox abilities. We and others have recently shown through chemical and electro-

dx.doi.org/10.1021/ja405284t | J. Am. Chem. Soc. 2013, 135, 14670−14678

Scheme 1. Observed Electron Transfer Conversions in 1

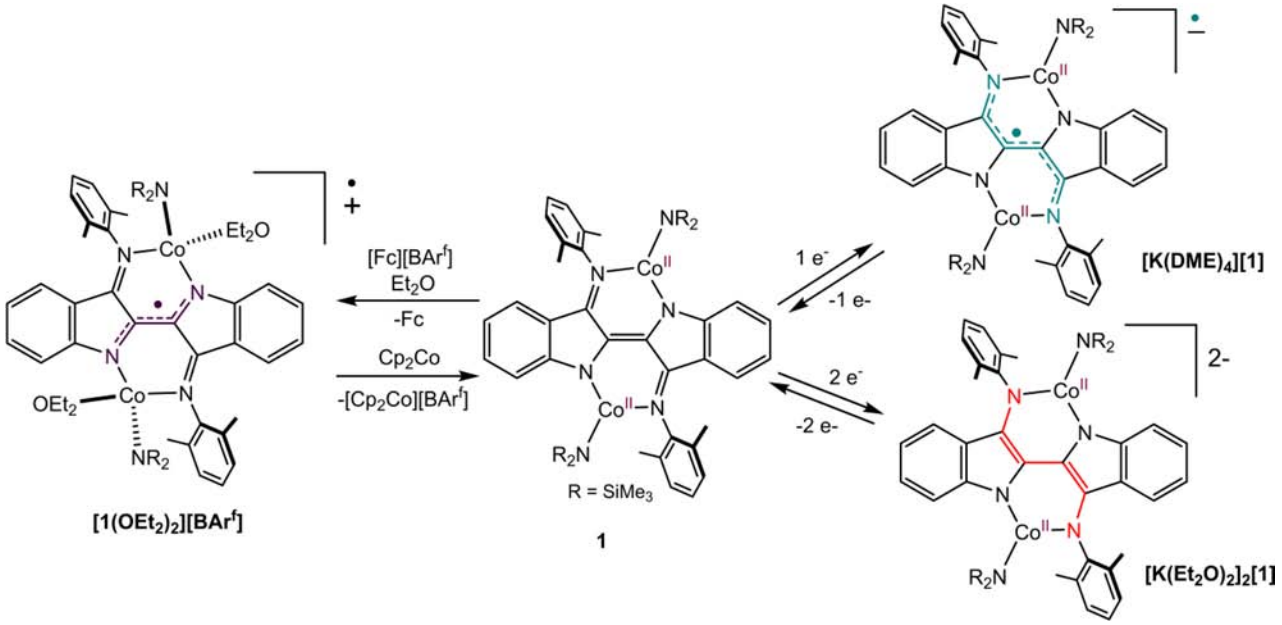

chemical methods the ability of nindigo to exist in five distinct oxidation states ranging from neutral dehydronindigo to a tetraanionic, closed-shell form on complexation to a metal (Scheme S1, Supporting Information).[12,24]

We were attracted to the unique redox activity of the nindigo system for use in coordination compounds with base metals, namely cobalt, to generate complexes capable of effecting multielectron chemical transformations, beyond the Co^{2+}/Co^{3+} redox couple.[25] Moreover, as high-spin cobalt(II) ($S = {}^3/_2$) possesses an intrinsic magnetic anisotropy,[3a,5] we were also interested in using nindigo to synthesize new bimetallic SMMs. Nindigo, with its β-diketiminate-type attributes, allows for control over the metal coordination environment, while its electronic properties, namely its highly conjugated framework, potentially provide a means to mediate metal−metal communication while also allowing for housing of electrons and electron holes.

We recently reported the synthesis of the paramagnetic dinuclear Co(II) nindigo complex $dmp_2Nin\{Co[N(SiMe_3)_2]\}_2$ (**1**) (dmp_2Nin = bis(2,6-dimethylphenyl)nindigo) possessing two trigonal-planar, high-spin metal centers.[12] The reported cyclic voltammogram (CV) of **1** displays two reversible cathodic waves corresponding to its isolable one- and two-electron reduction products $[K(DME)_4][dmp_2Nin\{Co[N(SiMe_3)_2]\}_2]$ ($[K(DME)_4][\mathbf{1}]$) and $[K(Et_2O)_2]_2[dmp_2Nin\{Co[N(SiMe_3)_2]\}_2]$ ($[K(Et_2O)_2]_2[\mathbf{1}]$), respectively (Scheme 1). Whereas $[K(Et_2O)_2]_2[\mathbf{1}]$ contains a tetraanionic, closed-shell nindigo ligand, complex $[K(DME)_4][\mathbf{1}]$ contains a trianionic nindigo radical. Slight but significant changes in the metrical parameters of the nindigo backbone reveal the radical of $[K(DME)_4][\mathbf{1}]$ to be delocalized throughout its conjugated 1,6-diazatriene moiety, thus sandwiching the ligand radical between the two $S = {}^3/_2$ cobalt centers (Scheme 1).

Notably, the CV trace of **1** also exhibits a reversible anodic wave at −0.12 V (referenced vs. $Cp_2Fe^{0/+}$ at 0.00 V), which we had assigned to a cationic species.[12] Indeed, treatment of a suspension of **1** in Et_2O with 1 equiv of the mild oxidizing agent $[Fc][BAr^f]$ (Fc = Cp_2Fe^+; BAr^f = $B(3,5\text{-}(CF_3)_2C_6H_3)_4$) generates the monocationic cobalt nindigo complex $[dmp_2Nin\{Co[N(SiMe_3)_2](OEt_2)\}_2][BAr^f]$ ($[\mathbf{1}(OEt_2)_2][BAr^f]$) in 74% isolated yield (Scheme 1) as a deep purple colored solid. $[\mathbf{1}(OEt_2)_2][BAr^f]$ is insoluble in arenes and nonpolar solvents but highly soluble in Et_2O. Its ^1H NMR spectrum in THF-d_8 displays broad resonances, between −20.2 and 119.3 ppm, revealing this species to be paramagnetic.

3.2. Structural Studies of Complex $[\mathbf{1}(OEt_2)_2][BAr^f]$. Since both cobalt and nindigo possess the potential for redox activity, the solid-state structure of $[\mathbf{1}(OEt_2)_2][BAr^f]$ was determined by X-ray crystallographic analysis to ascertain where the one-electron oxidation occurs. $[\mathbf{1}(OEt_2)_2][BAr^f]$ is comprised of noninteracting $[dmp_2Nin\{Co[N(SiMe_3)_2](Et_2O)\}_2]^+$ and $[BAr^f]^-$ units, with each Co center in the cationic fragment displaying a four-coordinate geometry (Figure 1). The asymmetric unit of $[\mathbf{1}(OEt_2)_2][BAr^f]$ contains two crystallographically independent half molecules of $[dmp_2Nin\{Co[N(SiMe_3)_2](Et_2O)\}_2]^+$, each lying on an inversion center, with the complete symmetry-generated cations sharing nearly identical metrical parameters. Unlike the trigonal-planar coordination geometries observed for the cobalt ion in complexes **1** (Table 1), $[K(DME)_4][\mathbf{1}]$, and $[K(Et_2O)_2]_2[\mathbf{1}]$, the binding of Et_2O to $[\mathbf{1}(OEt_2)_2][BAr^f]$ provides the cobalt with a distorted-tetrahedral geometry (e.g., N1−Co1−N2 = 93.73(6)°, N1−Co1−N3 = 114.64(7)°). The coordination of Et_2O to cobalt in $[\mathbf{1}(OEt_2)_2][BAr^f]$ is not unexpected, as **1** is known to also bind ethereal solvents.[12] All attempts to synthesize $[\mathbf{1}][BAr^f]$, free of coordinating solvent, have been unsuccessful.

Close inspection of the bond lengths in $[\mathbf{1}(OEt_2)_2]^+$ reveals minor structural changes associated with the nindigo ligand skeleton. For instance, the central nindigo C−C bond, which we have found to be highly sensitive to the ligand oxidation state, lengthens slightly in $[\mathbf{1}(OEt_2)_2]^+$ (C1−C1* = 1.410(3) Å) by ca. 0.02 Å over that found in neutral **1**.[12] Additionally, the $N_{pyrrolide}-C_{bridge}$ distance (N1−C1 = 1.348(2) Å) of $[\mathbf{1}(OEt_2)_2]^+$, anticipated to decrease upon ligand oxidation, shortens by a mere ca. 0.02 Å in comparison to the corresponding bond distance in **1**. Altogether, the subtle changes within the ligand backbone, while minimal, are

dx.doi.org/10.1021/ja405284t | J. Am. Chem. Soc. 2013, 135, 14670−14678

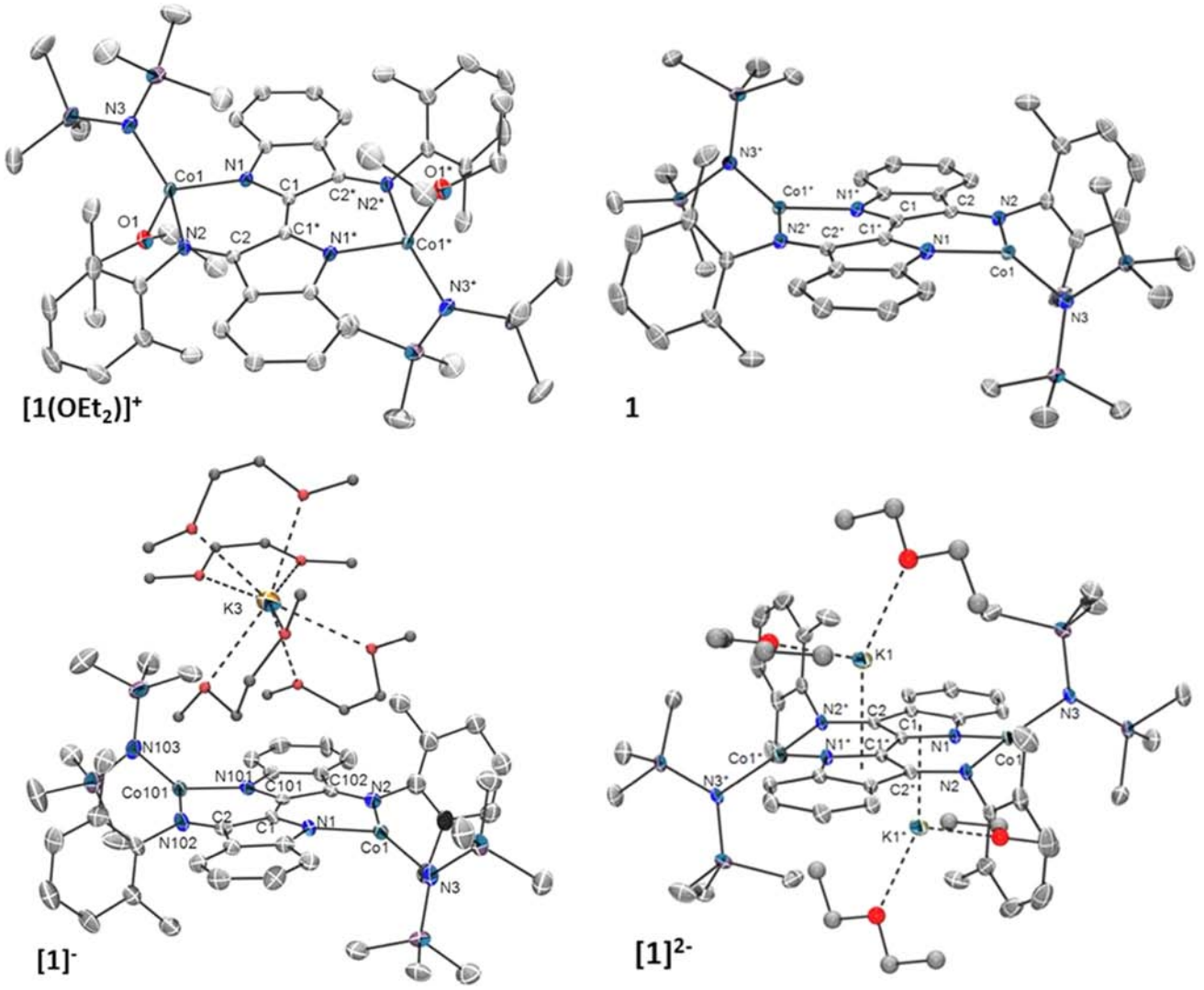

Figure 1. Solid-state molecular structures $[\mathbf{1}(OEt_2)]^+$, **1**, $[\mathbf{1}]^-$ and $[\mathbf{1}]^{2-}$ with 40% probability ellipsoids.[12] The anion for $[\mathbf{1}(OEt_2)_2][BAr^f]$ and all hydrogen atoms have been removed for clarity. Asterisks denote symmetry-generated atoms.

consistent with a largely delocalized, nindigo-centered radical monocation (cf. Scheme 1). Similar behavior has been observed in the related oxidized Ni(II) species $[Ni(nacnac)_2]^+$ (nacnac = 1,2,4,5-tetramethyl-β-diketiminate), which features nearly undetectable intraligand bond changes owing to radical delocalization through a conjugated system.[26] In accordance with the decreased formal charge of the nindigo ligand, both the $Co-N_{pyrrolide}$ (Co1–N1 = 1.978(2) Å) and $Co-N_{imine}$ (Co1–N2 = 2.005(2) Å) distances increase by ca. 0.05 Å while the $Co-N_{amide}$ (Co1–N3 = 1.916(2) Å) bond decreases by ca. 0.04 Å. Had oxidation been purely metal-based, a decrease in *both* the Co–amide and Co–nindigo bond lengths would be anticipated with little to no changes occurring within the ligand. Finally, the UV–vis–near-IR spectrum of $[\mathbf{1}(OEt_2)_2]^+$ exhibits a broad, low-intensity band at 973 nm. This band, absent in both **1** and $[K(Et_2O)_2]_2[\mathbf{1}]$, is suggestive of a charge transfer band affiliated with a nindigo ligand radical.[26,27] Indeed, a similar band has also been observed for the nindigo radical anion $[K(DME)_4][\mathbf{1}]$.[12]

The CV of $[\mathbf{1}(OEt_2)_2][BAr^f]$ in THF (Figure S6, Supporting Information) displays three reversible reduction waves at −0.17, −1.51, and −2.10 V mirroring those observed for **1** and its anionic derivatives.[12] Moreover, addition of 1 equiv of Cp_2Co, as a reducing agent, to $[\mathbf{1}(OEt_2)_2][BAr^f]$, in THF-$d_8$ cleanly regenerates the parent complex **1**, as indicated by ^1H NMR spectroscopy (Scheme 1; Figure S3, Supporting Information). As a result, such well-behaved chemical and electrochemical reversibility is consistent throughout the four-state series in $\mathbf{1}^n$ (n = 1+, 0, 1−, 2−).

We have also found some of these compounds to be robust. For instance, **1** can be sublimed at 160 °C under reduced pressure, while its reduced products $[K(DME)_4][\mathbf{1}]$ and solid $[K(Et_2O)_2]_2[\mathbf{1}]$ can be stored indefinitely at room temperature under an inert atmosphere. With the exception of $[\mathbf{1}(OEt_2)_2][BAr^f]$, which slowly decomposes over several hours upon standing in THF at room temperature, complexes **1**, $[K(DME)_4][\mathbf{1}]$, and $[K(Et_2O)_2]_2[\mathbf{1}]$ are indefinitely stable in solution and can be heated in toluene to at least 110 °C for several days without decomposing. Altogether, given (1) their stability and reversible redox switchability, (2) the presence of two high-spin Co(II) centers, and (3) the ability to sandwich stable ligand radicals between metals, potentially enhancing magnetic exchange coupling,[6a,c,8] make these materials attractive SMM candidates. Accordingly, their magnetic properties were investigated by SQUID magnetometry.

dx.doi.org/10.1021/ja405284t | J. Am. Chem. Soc. 2013, 135, 14670–14678

Table 1. Selected Bond Lengths (Å) and Angles (deg) for 1, $[1(OEt_2)_2]^+$, $[1]^-$, and $[1]^{2-}$ using the Skeleton Shown Below

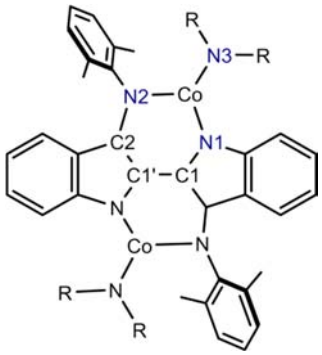

	$[1(OEt_2)_2]^+$	1	$[1]^-$	$[1]^{2-}$
C1–C1′	1.410(3)	1.393(2)	1.416(7)	1.438(3)
C2–N2	1.303(2)	1.321(1)	1.361(6)	1.401(2)
C1–C2	1.484(2)	1.466(1)	1.412(7)	1.404(2)
Co–N1	1.978(2)	1.9301(9)	1.934(4)	1.973(1)
Co–N2	2.005(2)	1.9569(8)	1.912(4)	1.901(1)
Co–N3	1.916(2)	1.8792(8)	1.914(4)	1.913(1)
Co–Co′	6.194	6.062	6.079	6.053
N1–Co–N2	93.73(6)	95.80(3)	95.3(3)	97.87(5)
N1–Co–N3	114.64(7)	126.42(4)	125.3(4)	120.82(5)
N2–Co–N3	125.94(7)	133.19(4)	136.5(4)	138.52(6)

3.3. Magnetic Data. In order to probe the magnetic properties of all complexes, direct current (dc) and alternating current (ac) susceptibility measurements were obtained with the use of a Quantum Design SQUID magnetometer.

The dc magnetic susceptibility measurements were carried out for all complexes in the 1.8–300 K temperature range and under a 0.1 T applied dc field (Figure 2). At room temperature, the χT product value of **1** is 5.50 cm^3 K mol^{-1}, which is higher than the expected spin-only value of 3.76 cm^3 K mol^{-1} for two noninteracting high-spin Co(II) ions (assuming $g = 2$). These values are, however, within the range of observed experimental values reported for Co(II) ions.[28] This feature simply indicates that there is significant magnetic anisotropy (which is common for Co(II) systems) that tends to give a larger magnetic moment at room temperature. Upon a decrease of the temperature, a gradual decrease of the χT product can be observed, which indicates the presence of dominant intramolecular antiferromagnetic interactions between the two trigonal-planar Co(II) ions. Such interactions are mediated by the neutral nindigo ligand acting as a superexchange pathway, which subsequently leads to a singlet spin ground state at below 1.8 K. Due to the highly anisotropic nature of Co(II) ions, it is not possible to fit the data using a Kambe's vector coupling method. Ab initio studies were performed to gain insight into the strength and nature of the magnetic interactions between the spin carriers, and these results will be presented and discussed in the computational section (vide infra).

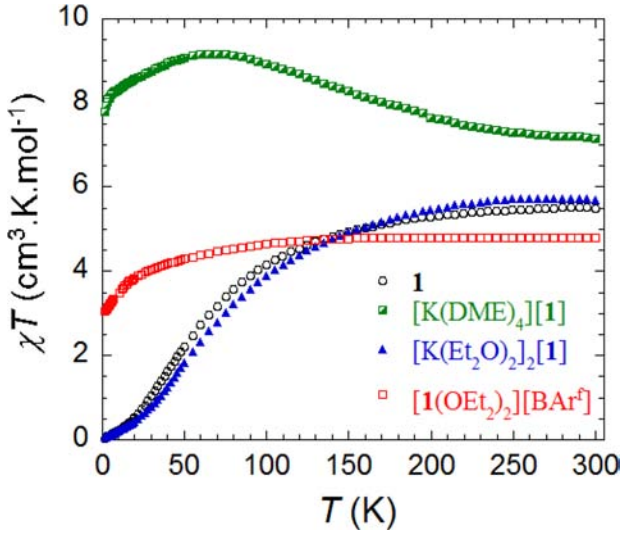

Figure 2. Temperature dependence of the χT product at 0.1 T for **1**, $[K(DME)_4][1]$, $[K(Et_2O)_2]_2[1]$, and $[1(OEt_2)_2][BAr^f]$ (with χ being the molar susceptibility per dinuclear complex defined as M/H).

Magnetization data below 8 K for **1** reveal (Figure S8, Supporting Information) a small magnetic moment indicative of a singlet ground state for the molecule, and the observed vanishing moment is most likely due to slightly populated excited states.

For the radical anion complex $[K(DME)_4][1]$ the observed χT value of 7.15 cm^3 K mol^{-1} is also higher than the anticipated spin-only value of 4.13 cm^3 K mol^{-1} for two noninteracting Co(II) ions and a radical anion ligand ($S = {}^1/_2$). This high-spin value could result from several factors, such as significant spin–orbit coupling inherent to the Co(II) ions as well as non-negligible intermolecular interactions even at room temperature. In $[K(DME)_4][1]$, the two trigonal-planar Co(II) ions are now bridged by a stable trianionic nindigo radical, and it is well-known that metal–radical magnetic interactions could be significant.[29] When the temperature is lowered, the χT product gradually increases to reach the maximum value of 9.15 cm^3. K mol^{-1} at 65 K before decreasing to a value of 7.80 cm^3 K mol^{-1} at 1.8 K. The observed increase of χT between 300 and 70 K is due to the presence of dominant ferromagnetic interactions between the spin carriers. Two possibilities can be envisioned, as shown in Scheme 2: (1) an overall ferromagnetic interaction

Scheme 2. Spin Alignment Possibilities between Co(II) (Green) and Radical (Black) Spin Centers

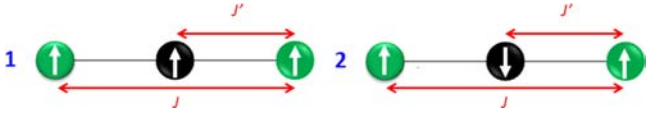

between all spin centers (cobalt(↑ = ${}^3/_2$)–radical(↑ = ${}^1/_2$)–cobalt(↑ = ${}^3/_2$)) leading to an overall $S = {}^7/_2$ ground state; (2) antiferromagnetic coupling between the Co(II) ions and radical ligand (cobalt(↑ = ${}^3/_2$)–radical(↓ = ${}^1/_2$)–cobalt(↑ = ${}^3/_2$)) leading to an $S = {}^5/_2$ ground state. If the latter is occurring, the increase in χT can be attributed to a parallel alignment of the spins on the Co(II), which suggests a strong coupling between the spins of the cobalt and the radical ligand. However, on the basis of the χT value at 300 K neither situation can be ruled out; therefore, to accurately elucidate the nature and strength of these interactions ab initio calculations were performed and the results will be discussed in the next section.

In the magnetization study of $[K(DME)_4][1]$, the M vs H data (Figure S9, Supporting Information) below 8 K reveal a rapid increase in the magnetization at low magnetic fields and at higher fields the curve gradually increases, followed by a

dx.doi.org/10.1021/ja405284t | J. Am. Chem. Soc. 2013, 135, 14670–14678

plateau indicating saturation. At the lowest temperature (1.8 K) and highest field (7 T), assuming only the ground state is populated, a saturation value of 5.55 μ_B suggests a ground state of $S = {}^5/_2$. In the M vs H/T data (Figure S9) the isotemperature lines do not fully superimpose on top of each other; this suggests non-negligible magnetic anisotropy is present in the molecule.

Complex $[K(Et_2O)_2]_2[\mathbf{1}]$ with a doubly reduced tetraanionic, closed-shell bridging nindigo ligand exhibits magnetic susceptibility behavior similar to that of **1**. Accordingly, the room-temperature χT value of 5.68 cm^3 K mol^{-1} resembles the value observed for **1**. The decrease of the χT product with decreasing temperature is indicative of a dominant antiferromagnetic interaction between the two Co(II) ions, leading to an overall $S = 0$ spin ground state. It is remarkable to observe that the shape of the overall susceptibility curve for $[K(Et_2O)_2]_2[\mathbf{1}]$ is very similar to that observed for **1**, confirming the closed-shell nature of the nindigo ligand in both systems. Moreover, and as in **1**, small magnetic moments observed in magnetization data (Figure S15, Supporting Information) confirm the singlet ground state due to the antiferromagnetic coupling between the Co(II) ions.

In the monocationic cobalt nindigo complex $[\mathbf{1}(OEt_2)_2][BAr^f]$ the two Co(II) ions each adopt a tetrahedral geometry due to coordination of OEt_2, and each Co(II) ion is bridged by a nindigo radical monocation. The room-temperature χT value of 4.79 cm^3 K mol^{-1} is lower than the values observed for **1** and $[K(DME)_4][\mathbf{1}]$. When the temperature is lowered, the χT product decreases gradually and reaches a minimum value of 3.04 cm^3 K mol^{-1} at 1.8 K. Such negative deviation is generally indicative of dominant antiferromagnetic interactions; however, significant magnetic anisotropy could also mask the interactions and lead to similar behavior.[30] The negative deviation of the χT product can easily be observed in a highly anisotropic mononuclear cobalt complex.[30]

Divalent cobalt complexes are known to possess large magnetic anisotropy.[5,31] The octahedral complexes tend to exhibit significant first-order orbital angular momentum thanks to an accessible ^4T state. Among these, only a handful of cobalt complexes with unusual coordination environments have exhibited unique magnetic properties.[28a,32] Although an octahedral ligand field is predicted to be ideal for harnessing large anisotropy in metal ions, recent studies demonstrate complexes in low coordination environments can in fact exhibit significant spin−orbit coupling.[32b] To our knowledge in-depth magnetic properties of trigonal-planar Co(II) complexes have yet to be reported.[32c] Therefore, to investigate the dynamic susceptibility of all four complexes, ac susceptibility measurements were carried out for the radical anion and radical cation. For the complexes **1** and $[K(Et_2O)_2]_2[\mathbf{1}]$ no ac signal was observed, precluding any slow magnetic relaxation. This is consistent with the observation of a singlet ground state ($S = 0$), which leads to an absence of an energy barrier ($\Delta E = S^2|D| = 0$).

For $[K(DME)_4][\mathbf{1}]$, however, an ac susceptibility signal was observed under the aforementioned conditions (Figure S10, Supporting Information), indicating SMM behavior. No peak maxima were observed in the out-of-phase plot (imaginary component of the dynamic susceptibility, Figure S10 bottom); therefore, no relaxation time can be extracted. Such behavior most likely results from quantum tunneling of the magnetization (QTM). Kramers theory predicts the ground state QTM (between the ground $\pm M_S$ or $\pm M_J$ levels) is minimized due to the spin-parity effect for half-integer spin systems,; however, this can occur experimentally due to several variables such as hyperfine/dipolar coupling via transverse field compounds as well as environmental degrees of freedom.[32]

Experimentally, QTM can be reduced by applying a static dc field, which lifts the degeneracy. Under applied dc fields, frequency-dependent ac signals were observed for $[K(DME)_4][\mathbf{1}]$, with peak maxima confirming its SMM behavior. This enhancement of peak intensity/signal clearly indicates significant quantum tunneling of the magnetization (QTM) in this molecule. In order to reduce this QTM, a measurement was performed to identify the optimum field. These measurements resulted in the observation of multiple relaxation pathways occurring in $[K(DME)_4][\mathbf{1}]$ (Figure S10). Subsequently, ac measurements under 1200 and 6000 Oe were carried out in order to further probe the occurring relaxation mechanisms. A full frequency-dependent signal was observed in the out-of-phase plot (Figure 3) and under an applied optimum field QTM is minimized.

From the data measured at 1200 Oe a graphical representation (Cole−Cole[33]) of χ'' *vs* χ' produced large semicircles. These data are in good agreement with the

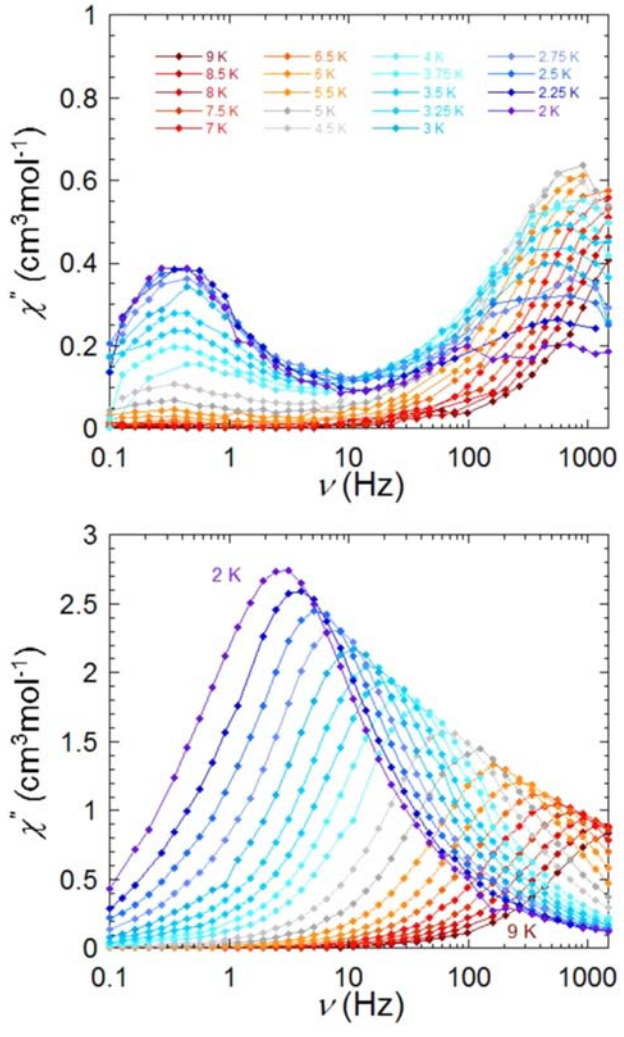

Figure 3. Out-of phase (χ'') ac susceptibility from 2 to 9 K under static applied dc fields of 1200 (top) and 6000 Oe (bottom) for $[K(DME)_4][\mathbf{1}]$.

dx.doi.org/10.1021/ja405284t | J. Am. Chem. Soc. 2013, 135, 14670−14678

generalized Debye model[34] (α values range 0.08−0.27), indicating the magnetic susceptibility is unique to a single relaxation process (Figure S13, Supporting Information). A relaxation barrier of 33 K with $\tau_0 = 2.2 \times 10^{-6}$ s was obtained from frequency-dependent data using an Arrhenius equation ($\tau = \tau_0 \exp(\Delta E/k_B T)$ (Figure S14, Supporting Information). Although this value is comparatively low, it is able to successfully demonstrate that coupling metal centers through switchable ligands can control not only alignment of the spin but *can also turn on SMM behavior*. Measurements carried out under a larger static dc field of 6000 Oe now exhibit two clear peaks with maxima located at different frequencies. The occurrence of such peaks is indicative of field-induced SMM behavior in $[K(DME)_4][\mathbf{1}]$ with multiple relaxation pathways which can be accessed through different applied fields. The Cole−Cole plot confirms several relaxation pathways by the occurrence of multiple semicircles in the χ' *vs* χ'' representation (Figure S16, Supporting Information). Temperature-dependent shifting peak maxima between 100 and 1500 Hz can be associated with a slow relaxation mechanism, while the less prominent peaks at low frequencies (0.1−10 Hz) can be associated with relatively fast relaxation of the magnetization. It is noteworthy that the absence of a clear shift in the peaks suggests a relaxation through a new thermally activated QTM pathway accessed via this applied field.

Akin to the case for $[K(DME)_4][\mathbf{1}]$, the oxidized derivative of **1**, $[\mathbf{1}(OEt_2)_2][BAr^f]$, displays a frequency-dependent ac signal at zero field; however, no full peak was observed in the χ'' vs frequency plot (Figure S19, Supporting Information). For $[\mathbf{1}(OEt_2)_2][BAr^f]$, an optimum field of 1200 Oe was found to be ideal to reduce QTM. Our ac data under this field reveals a full frequency dependent peak between 4.2 and 1.8 K indicative of field-induced SMM behavior (Figure 4). Cole−Cole analysis

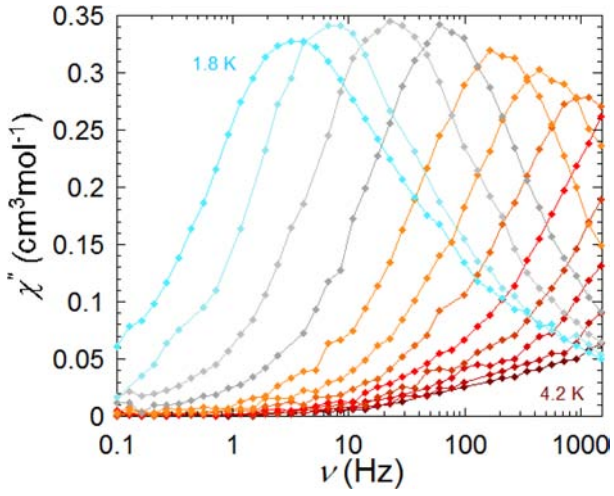

Figure 4. Frequency dependence of the out of phase (χ'') ac susceptibility from 1.8 to 4.2 K under a 1200 Oe applied dc field for $[\mathbf{1}(OEt_2)_2][BAr^f]$.

confirms only one relaxation process under the optimum field, with α values of 0.16−0.42 (Figure S21, Supporting Information). The Arrhenius equation yielded a relaxation barrier of 37 K with $\tau_0 = 1 \times 10^{-9}$ s. The obtained relaxation barrier is slightly higher than that observed for $[K(DME)_4][\mathbf{1}]$; however, with a small pre-exponential factor (τ_0). The small difference in slow magnetization relaxation behavior between $[K(DME)_4][\mathbf{1}]$ and $[\mathbf{1}(OEt_2)_2][BAr^f]$ is most likely the result of the local anisotropy difference in trigonal-planar versus tetrahedral geometries in cobalt(II) ions.

3.4. Theoretical Investigations. The best agreement of the magnetic susceptibility and magnetization of complexes **1** and $[K(Et_2O)_2]_2[\mathbf{1}]$ were obtained within the basis set α (Table S3, Supporting Information) for the CASPT2 calculations. For the complexes $[K(DME)_4][\mathbf{1}]$ and $[\mathbf{1}(OEt_2)_2][BAr^f]$ the CASPT2 calculations were not performed because they did not give much change in the energies for **1** and $[K(Et_2O)_2]_2[\mathbf{1}]$. In the simulation of magnetism of $[K(DME)_4][\mathbf{1}]$ we used the ab initio results obtained within basis set α/fragment A, while for the complex $[\mathbf{1}(OEt_2)_2]$-$[BAr^f]$ the results from basis set β/fragment B were utilized. The χT *vs* T curves and the magnetization curves were simulated using the POLY_ANISO module and are shown in Figures S23−S26 (Supporting Information).

1. From the experimental data it is apparent that the two cobalt ions are coupled antiferromagnetically. The best fitting was provided by the exchange coupling constant between two Co(II) ions of −11.7 cm^{-1}. Complexes with similar coupling constants are known for nonradical bridged systems.[35] The lowest exchange doublet is nonmagnetic (all g factors within it are 0); therefore, this complex cannot be an SMM. The separation between the levels of this doublet (tunneling splitting) is 1.3 cm^{-1}.

$[K(Et_2O)_2]_2[\mathbf{1}]$. This complex exhibits almost the same magnetic behavior as **1**. Considering the two ligand radicals as being coupled strongly antiferromagnetically (and because $S_{nindigo}$ = 0, closed shell), we included in the magnetic simulations only the exchange interaction between the cobalt sites. The value of −14.7 cm^{-1} for this exchange coupling constant was found to give the best fit. The ground exchange doublet of this complex is also nonmagnetic. Therefore, as in the preceding case, this complex cannot be a SMM, and the tunneling gap within the ground exchange doublet is 2.7 cm^{-1}.

$[K(DME)_4][\mathbf{1}]$. Fragment ab initio calculations have been performed for the corresponding neutral complex **1**. Nevertheless, for the simulation of magnetism an isotropic spin $S = {}^1/_2$ of the nindigo radical has been added to the model. The best fitting of the magnetic susceptibility was obtained by assuming a ferromagnetic interaction between cobalt ions and an antiferromagnetic interaction between Co and the radical. The fitted exchange coupling constants are +14.51 cm^{-1} between the cobalt ions and −132.74 cm^{-1} between Co ion and radical, respectively. The strong interactions between the cobalt ion and nindigo radical are slightly higher than reported coupling constants for other radicals and Co(II) ions.[35] This strong antiferromagnetic coupling dictates the parallel alignment of the spin vectors between the two cobalt ions in this case. Recently, Murray et al. reported a monomeric cobalt nitroxide complex in which strong ferromagnetic exchange interaction was observed due to a polarization mechanism.[36] A similar exchange pathway could also be the origin of such strong magnetic interaction between the Co(II) ion and radical ligand here. The ground exchange state of this compound is a magnetic Kramers doublet. The main values of its g tensors are 0.3, 0.6, and 16.9. Thus, the ground doublet is quite axial. However, due to non-negligible transverse g factors (0.3 and 0.6), the QTM is not quenched in this compound. As a result, this species shows SMM behavior (maximum of out-of-phase magnetic susceptibility) only in the presence of an applied dc magnetic field.

dx.doi.org/10.1021/ja405284t | J. Am. Chem. Soc. 2013, 135, 14670−14678

[1(OEt$_2$)$_2$][BAr^f]. As in the previous complex, fragment calculations of spin−orbital multiplets on the Co(II) sites have been performed for the neutral complex **1** (Table S4, Supporting Information), while the spin of the radical was taken into account at the stage of simulations of the magnetism. The best fitting of the χT data was obtained within the following exchange coupling parameters: J(Co−Co) = −10 cm^{-1} and J(Co−nindigo radical) = −30 cm^{-1}. However, our calculated $M(H)$ value deviates strongly from the experimental curve. Moreover, this set of exchange parameters predicts relatively large values of the transverse g factors in the ground exchange doublet: g_x = 1.3 and g_y = 1.7. These large values cannot explain the SMM behavior of this compound even in an applied dc field. Keeping in mind that the cobalt−nindigo interaction in the complex [K(DME)$_4$][**1**] was found to be very strong, we may assume that in the complex [**1**(OEt$_2$)$_2$][BAr^f] the cobalt−radical interaction might be of comparable strength. Fitting the magnetization curve under the assumption of a strong antiferromagnetic interaction between cobalt and nindigo, we found a better set of exchange coupling constants: J(Co−Co) = −3.5 cm^{-1} and J(Co−nindigo) = −138 cm^{-1}. For these exchange parameters the main values of the g tensors are 0.08, 0.09, and 12.3. The small values of transverse g factors are in accord with the observed SMM behavior of [**1**(OEt$_2$)$_2$][BAr^f]. Furthermore, the obtained values of g_x and g_y are even smaller than in [K(DME)$_4$][**1**], justifying why the radical cation is a better SMM (i.e., possesses a higher relaxation barrier, uniaxiality of the anisotropy) than its radical anionic form, [**1**]$^-$ (cf. Figures S14 and S19 in the Supporting Information for relaxation times of [K(DME)$_4$][**1**] and [**1**(OEt$_2$)$_2$][BAr^f], respectively).

4. CONCLUSION

A fully reversible magnetic switch is presented where SMM behavior is turned "ON/OFF" by utilizing the redox behavior of a nindigo ligand bridging two Co(II) ions, by virtue of removing or adding an electron. The Co(II) ions, each possessing a spin of $^3/_2$, are coupled antiferromagnetically in complex **1** and [K(Et$_2$O)$_2$]$_2$[**1**], as demonstrated by the observed singlet ground state and confirmed by the calculated nonmagnetic lowest exchange doublet. Conversely, the complexes [K(DME)$_4$][**1**] and [**1**(OEt$_2$)$_2$][BAr^f] exploit a Co(II)−nindigo radical−Co(II) arrangement where net ferromagnetic interaction between metal centers results from strong antiferromagnetic interaction between each Co(II) and the radical, leading to the observed SMM behavior. Our study targeted redox-active ligands to demonstrate a molecular scale magnetic switch utilizing SMMs. By exploiting different metals (i.e. lanthanides, actinides, etc.) and strategic ligand design, redox-controllable magnetic switches can be tailored to a wide range of specific technical applications in intelligent materials, including molecular spintronics.

■ ASSOCIATED CONTENT

Supporting Information

Figures, tables, and a CIF files giving a detailed description of the computation data, packing diagrams, infrared data and crystallographic data. This material is available free of charge via the Internet at http://pubs.acs.org.

■ AUTHOR INFORMATION

Corresponding Authors

M.Murugesu@uottawa.ca
Liviu.Chibotaru@chem.kuleuven.be
mindiola@indiana.edu and mindiola@sas.upenn.edu
caulton@indiana.edu

Present Address

[‖]Department of Chemistry, University of Pennsylvania, 231 South 34th Street, Philadelphia, Pennsylvania 19104, United States.

Notes

The authors declare no competing financial interest.

■ ACKNOWLEDGMENTS

This work has been supported in large part by the National Science Foundation American Competitiveness in Chemistry Fellowship (S.F.; CHE-1137284). We also thank the University of Ottawa, CCRI, NSERC (Discovery and RTI grants), Early Researcher Award, Vision 2010, CFI, ORF, and FFCR for their support.

■ REFERENCES

(1) Sessoli, R.; Gatteschi, D.; Caneschi, A.; Novak, M. A. *Nature* **1993**, *365*, 141.

(2) (a) Leuenberger, M. N.; Loss, D. *Nature* **2001**, *410*, 789. (b) Cavallini, M.; Facchini, M.; Albonetti, C.; Biscarini, F. *Phys. Chem. Chem. Phys.* **2008**, *10*, 784.

(3) (a) Jurca, T.; Farghal, A.; Lin, P. H.; Korobkov, I.; Murugesu, M.; Richeson, D. S. *J. Am. Chem. Soc.* **2011**, *133*, 15814. (b) Jeon, I.-R.; Clerac, R. *Dalton Trans.* **2012**, *41*, 9569.

(4) (a) Long, J. R. Molecular Cluster Magnets. In *The Chemistry Of Nanostructured Materials*; Yang, P., Ed.; World Scientific: Hong Kong, 2003; p 291. (b) Freedman, D. E.; Jenkins, D. M.; Iavarone, A. T.; Long, J. R. *J. Am. Chem. Soc.* **2008**, *130*, 2884.

(5) Murrie, M. *Chem. Soc. Rev.* **2010**, *39*, 1986.

(6) (a) Habib, F.; Murugesu, M. *Chem. Soc. Rev.* **2013**, *42*, 3278. (b) Le Roy, J. J.; Jeletic, M.; Gorelsky, S. I.; Korobkov, I.; Ungur, L.; Chibotaru, L. F.; Murugesu, M. *J. Am. Chem. Soc.* **2013**, *135*, 3502. (c) Demir, S.; Zadrozny, J. M.; Nippe, M.; Long, J. R. *J. Am. Chem. Soc.* **2012**, *134*, 18546.

(7) (a) Harman, W. H.; Harris, T. D.; Freedman, D. E.; Fong, H.; Chang, A.; Rinehart, J. D.; Ozarowski, A.; Sougrati, M. T.; Grandjean, F.; Long, G. J.; Long, J. R.; Chang, C. J. *J. Am. Chem. Soc.* **2010**, *132*, 18115. (b) Freedman, D. E.; Harman, W. H.; Harris, T. D.; Long, G. J.; Chang, C. J.; Long, J. R. *J. Am. Chem. Soc.* **2010**, *132*, 1224. (c) Mossin, S.; Tran, B. L.; Adhikari, D.; Pink, M.; Heinemann, F. W.; Sutter, J.; Szilagyi, R. K.; Meyer, K.; Mindiola, D. J. *J. Am. Chem. Soc.* **2012**, *134*, 13651.

(8) (a) Rinehart, J. D.; Fang, M.; Evans, W. J.; Long, J. R. *Nat. Chem.* **2011**, *3*, 538. (b) Rajeshkumar, T.; Rajaraman, G. *Chem. Commun.* **2012**, *48*, 7856.

(9) (a) Miyasaka, H.; Yamashita, M. *Dalton Trans.* **2007**, 399. (b) Haryono, M.; Kalisz, M.; Sibille, R.; Lescouezec, R.; Fave, C.; Trippe-Allard, G.; Li, Y.; Seuleiman, M.; Rousseliere, H.; Balkhy, A. M.; Lacroix, J.-C.; Journaux, Y. *Dalton Trans.* **2010**, *39*, 4751. (c) Morimoto, M.; Miyasaka, H.; Yamashita, M.; Irie, M. *J. Am. Chem. Soc.* **2009**, *131*, 9823.

(10) Freedman, D. E.; Jenkins, D. M.; Iavarone, A. T.; Long, J. R. *J. Am. Chem. Soc.* **2008**, *130*, 2884.

(11) Chávez, I.; Alvarez-Carena, A.; Molins, E.; Roig, A.; Maniukiewicz, W.; Arancibia, A.; Arancibia, V.; Brand, H.; Manuel Manríquez, J. *J. Organomet. Chem.* **2000**, *601*, 126.

(12) Fortier, S.; Moral, O. G.-d.; Chen, C.-H.; Pink, M.; Le Roy, J. J.; Murugesu, M.; Mindiola, D. J.; Caulton, K. G. *Chem. Commun.* **2012**, *48*, 11082.

(13) *SMART Apex II, Version 2.1*; Bruker AXS Inc., Madison, WI.

(14) *SAINT Version 7.34a*; Bruker AXS Inc.: Madison, WI.

(15) Blessing, R. *Acta Crystallogr. Sect. A: Found. Crystallogr.* **1995**, *A51*.

(16) Sheldrick, G. M. *SHELXTL, Version 6.12*; Bruker Analytical X-Ray Systems, Inc., Madison, WI.
(17) Aquilante, F.; De Vico, L.; Ferré, N.; Ghigo, G.; Malmqvist, P.-å.; Neogrády, P.; Pedersen, T. B.; Pitoňák, M.; Reiher, M.; Roos, B. O.; Serrano-Andrés, L.; Urban, M.; Veryazov, V.; Lindh, R. *J. Comput. Chem.* **2010**, *31*, 224.
(18) Roos, B. O.; Taylor, P. R.; Siegbahn, P. E. M. *Chem. Phys.* **1980**, *48*, 157.
(19) Andersson, K.; Malmqvist, P.-A.; Roos, B. O. *J. Chem. Phys.* **1992**, *96*, 1218.
(20) Andersson, K.; Roos, B. O. *Chem. Phys. Lett.* **1992**, *191*, 507.
(21) See the MOLCAS manual: http://molcas.org/documentation/manual/node95.html.
(22) Chibotaru, L. F.; Ungur, L.; Aronica, C.; Elmoll, H.; Pilet, G.; Luneau, D. *J. Am. Chem. Soc.* **2008**, *130*, 12445.
(23) Bourget-Merle, L.; Lappert, M. F.; Severn, J. R. *Chem. Rev.* **2002**, *102*, 3031.
(24) (a) Nawn, G.; Waldie, K. M.; Oakley, S. R.; Peters, B. D.; Mandel, D.; Patrick, B. O.; McDonad, R.; Hicks, R. G. *Inorg. Chem.* **2011**, *50*, 9826. (b) Oakley, S. R.; Nawn, G.; Waldie, K. M.; MacInnis, T. D.; Patrick, B. O.; Hicks, R. G. *Chem. Commun.* **2010**, *46*, 6753.
(25) Munha, R. F.; Zarkesh, R. A.; Heyduk, A. F. *Dalton Trans.* **2013**, *42*, 3751.
(26) Khusniyarov, M. M.; Bill, E.; Weyhermüller, T.; Bothe, E.; Wieghardt, K. *Angew. Chem., Int. Ed.* **2011**, *50*, 1652.
(27) (a) Scarborough, C. C.; Lancaster, K. M.; DeBeer, S.; Weyhermuller, T.; Sproules, S.; Wieghardt, K. *Inorg. Chem.* **2012**, *51*, 3718. (b) Dunn, T. J.; Ramogida, C. F.; Simmonds, C.; Paterson, A.; Wong, E. W.; Chiang, L.; Shimazaki, Y.; Storr, T. *Inorg. Chem.* **2011**, *50*, 6746.
(28) (a) Zadrozny, J. M.; Long, J. R. *J. Am. Chem. Soc.* **2011**, *133*, 20732. (b) Zheng, Y.-Z.; Tong, M.-L.; Zhang, W.-X.; Chen, X.-M. *Angew. Chem., Int. Ed.* **2006**, *45*, 6310.
(29) Sullivan, D. J.; Clerac, R.; Jennings, M.; Lough, A. J.; Preuss, K. E. *Chem. Commun.* **2012**, *48*, 10963.
(30) Zadrozny, J. M.; Telser, J.; Long, J. R. *Polyhedron* **2013**, DOI: 10.1016/j.poly.2013.04.008.
(31) Karasawa, S.; Zhou, G.; Morikawa, H.; Koga, N. *J. Am. Chem. Soc.* **2003**, *125*, 13676.
(32) (a) Vallejo, J.; Castro, I.; Ruiz-García, R.; Cano, J.; Julve, M.; Lloret, F.; De Munno, G.; Wernsdorfer, W.; Pardo, E. *J. Am. Chem. Soc.* **2012**, *134*, 15704. (b) Gomez-Coca, S.; Cremades, E.; Aliaga-Alcalde, N.; Ruiz, E. *J. Am. Chem. Soc.* **2013**, *135*, 7010. (c) Holland, P. L.; Cundari, T. R.; Perez, L. L.; Eckert, N. A.; Lachicotte, R. J. *J. Am. Chem. Soc.* **2002**, *124*, 14416.
(33) (a) Cole, K. S.; Cole, R. H. *J. Chem. Phys.* **1941**, *9*, 341. (b) Aubin, S. M. J.; Sun, Z.; Pardi, L.; Krzystek, J.; Folting, K.; Brunel, L. J.; Rheingold, A. L.; Christou, G.; Hendrickson, D. N. *Inorg. Chem.* **1999**, *38*, 5329.
(34) Gatteschi, D.; Sessoli, R.; Villain, J. *Molecular Nanomagnets*; Oxford University Press: Oxford, U.K., 2006.
(35) (a) Kurahashi, T.; Fujii, H. *Inorg. Chem.* **2013**, *52*, 3908. (b) Mitsumoto, K.; Shiga, T.; Nakano, M.; Nihei, M.; Nishikawa, H.; Oshio, H. *Eur. J. Inorg. Chem.* **2008**, *2008*, 4851. (c) Verani, C. N.; Gallert, S.; Bill, E.; Weyhermuller, T.; Wieghardt, K.; Chaudhuri, P. *Chem. Commun.* **1999**, 1747. (d) Petit, S.; Pilet, G.; Luneau, D.; Chibotaru, L. F.; Ungur, L. *Dalton Trans.* **2007**, *0*, 4582. (e) Zhang, Y.-Z.; Wernsdorfer, W.; Pan, F.; Wang, Z.-M.; Gao, S. *Chem. Commun.* **2006**, 3302. (f) Zhao, Q. H.; Tang, D. Y.; Zhang, Y. H.; Fang, R. B. *Russ. J. Coord. Chem.* **2006**, *32*, 261.
(36) Gass, I. A.; Tewary, S.; Nafady, A.; Chilton, N. F.; Gartshore, C. J.; Asadi, M.; Lupton, D. W.; Moubaraki, B.; Bond, A. M.; Boas, J. F.; Guo, S.-X.; Rajaraman, G.; Murray, K. S. *Inorg. Chem.* **2013**, *52*, 7557.